EUROPEAN ORGANIZATION FOR NUCLEAR RESEARCH

Search for K^+ decays into the $\pi^+ e^+ e^- e^+ e^-$ final state

The NA62 Collaboration

Abstract

The first search for ultra-rare K^+ decays into the $\pi^+ e^+ e^- e^+ e^-$ final state is reported, using a dataset collected by the NA62 experiment at CERN in 2017–2018. An upper limit of 1.4×10^{-8} at 90% CL is obtained for the branching ratio of the $K^+ \to \pi^+ e^+ e^- e^+ e^-$ decay, predicted in the Standard Model to be $(7.2 \pm 0.7) \times 10^{-11}$. Upper limits at 90% CL are obtained at the level of 10^{-9} for the branching ratios of two prompt decay chains involving pair-production of hidden-sector mediators: $K^+ \to \pi^+ aa$, $a \to e^+ e^-$ and $K^+ \to \pi^+ S$, $S \to A'A'$, $A' \to e^+ e^-$.

Introduction

Dark-sector models provide plausible dark-matter candidates, and represent a compelling new-physics direction to explore in its own right [1, 2]. So far, searches for the production of dark-sector mediators in meson decays have been focused on the production of a single particle, which is either invisible or decays into lepton or photon pairs. However, the parameter space of minimal dark sectors not yet excluded by experiment accommodates detectable pair-production of dark states [3, 4]. In the kaon sector, the process of particular interest is $K \to \pi X X$ followed by prompt $X \to e^+e^-$ decays, leading to characteristic multi-electron final states. Since this process has not been studied experimentally so far, $\mathcal{O}(10^{-6})$ sensitivity to its branching ratio is sufficient to improve existing constraints on dark-sector models.

The principal K^+ decay channel leading to the $\pi^+e^-e^-e^+e^-$ final state is the $K^+ \to \pi^+\pi^0$ decay followed by the double Dalitz decay $\pi^0_{\mathrm{DD}} \to e^+e^-e^+e^-$. This decay chain, denoted $K_{2\pi\mathrm{DD}}$, with a measured branching ratio of $(6.9\pm0.3)\times10^{-6}$ [5], is used for normalisation in this analysis. The non-resonant part of the $K^+ \to \pi^+e^+e^-e^+e^-$ decay, denoted $K_{\pi 4e}$, is expected to occur via one-photon ($K^+ \to \pi^+\gamma^*$) and two-photon ($K^+ \to \pi^+\gamma^*\gamma^*$) exchange with an expected Standard Model (SM) branching ratio of $(7.2 \pm 0.7) \times 10^{-11}$ [6]. The resulting final state is of two-fold interest in the context of dark sectors:

- A short-lived QCD axion (a) decaying into an e^+e^- pair is not completely ruled out by experiment [7, 8, 9], and provides a plausible explanation for the "17 MeV anomaly" in the mass spectra of the e^+e^- pairs produced in the de-excitation of ^{8}Be [10], ^{4}He [11] and ^{12}C [12] nuclei. Assuming an axion mass of 17 MeV/c^2, lower bounds of $\mathcal{B}(K_L \to \pi^0 aa) > 10^{-7}$ and $\mathcal{B}(K^+ \to \pi^+ aa) > 2 \times 10^{-8}$ (differing by the K_L/K^+ lifetime ratio) are predicted [3], allowing a test of the QCD axion explanation for the 17 MeV anomaly.

- A scenario involving a dark scalar (S), and a dark photon (A') with masses satisfying the condition $m_S \geq 2m_{A'}$ leads to a prompt cascade process $K^+ \to \pi^+S$, $S \to A'A'$ [3]. The case of prompt $A' \to e^+e^-$ decay leads to the same final state as the $K_{\pi 4e}$ decay.

The NA62 experiment at CERN collected a dataset of K^+ decays into final states containing lepton pairs in 2017–2018. The first search, performed using this dataset, is reported here for the $K_{\pi 4e}$ decay, and for pair-production of hidden-sector mediators in the prompt decay chains $K^+ \to \pi^+aa$, $a \to e^+e^-$ (denoted $K_{\pi aa}$) and $K^+ \to \pi^+S$, $S \to A'A'$, $A' \to e^+e^-$ (denoted $K_{\pi S}$).

1   Beam, detector and data sample

The layout of the NA62 beamline and detector [13] is shown schematically in Fig. 1. An unseparated secondary beam of π^+ (70%), protons (23%) and K^+ (6%) is created by directing 400 GeV/c protons extracted from the CERN SPS onto a beryllium target in spills of 3 s effective duration. The central beam momentum is 75 GeV/c, with a momentum spread of 1% (rms).

Beam kaons are tagged with a 70 ps time resolution by a differential Cherenkov counter (KTAG) that uses nitrogen gas at 1.75 bar pressure contained in a 5 m long vessel as the radiator. Beam particle positions, momenta and times are measured by a silicon pixel spectrometer consisting of three stations (GTK1,2,3) and four dipole magnets forming an achromat; a toroidal muon sweeper (scraper, SCR) is installed between GTK1 and GTK2. A 1.2 m thick steel collimator (COL) with a 76×40 mm^2 central aperture and 1.7×1.8 m^2 outer dimensions is placed upstream of GTK3 to absorb hadrons from upstream K^+ decays; a variable-aperture collimator of 0.15×0.15 m^2 outer dimensions was used up to early 2018. A dipole magnet (TRIM5) providing a 90 MeV/c horizontal momentum kick is located in front of GTK3. Inelastic interactions of beam particles in GTK3 are detected by an array of scintillator hodoscopes (CHANTI). The beam is delivered into a vacuum tank evacuated to 10^{-6} mbar, which contains a 75 m long
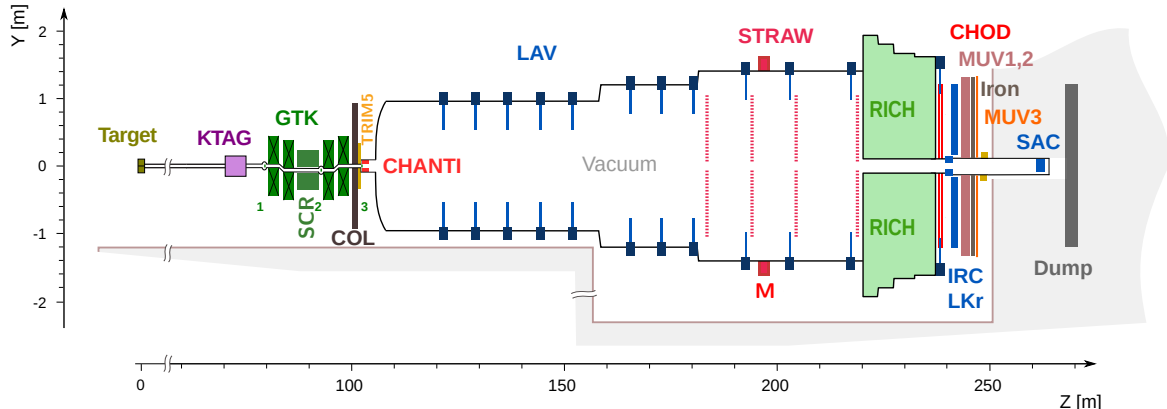
Figure 1: Schematic side view of the NA62 beamline and detector used in 2018.

fiducial volume (FV) starting 2.6 m downstream of GTK3. The beam angular spread at the FV entrance is 0.11 mrad (rms) in both horizontal and vertical planes. Downstream of the FV, undecayed beam particles continue their path in vacuum.

Momenta of charged particles produced in K^+ decays in the FV are measured by a magnetic spectrometer (STRAW) located in the vacuum tank downstream of the FV. The spectrometer consists of four tracking chambers made of straw tubes, and a dipole magnet (M) located between the second and third chambers that provides a horizontal momentum kick of 270 MeV/c in a direction opposite to that produced by TRIM5. The momentum resolution is $\sigma_p/p = (0.30 \oplus 0.005 \cdot p)\%$, with the momentum p expressed in GeV/c.

A ring-imaging Cherenkov detector (RICH) consisting of a 17.5 m long vessel filled with neon at atmospheric pressure provides particle identification, charged particle time measurements with a typical resolution of 70 ps, and the trigger time. Two scintillator hodoscopes (CHOD), which include a matrix of tiles and two planes of slabs arranged in four quadrants located downstream of the RICH, provide trigger signals and time measurements with 200 ps precision.

A $27X_0$ thick quasi-homogeneous liquid-krypton (LKr) electromagnetic calorimeter is used for particle identification and photon detection. The calorimeter has an active volume of 7 m³, segmented in the transverse direction into 13248 projective cells of 2×2 cm² size, and provides an energy resolution $\sigma_E/E = (4.8/\sqrt{E} \oplus 11/E \oplus 0.9)\%$, with E expressed in GeV. To achieve hermetic acceptance for photons emitted in K^+ decays in the FV at angles up to 50 mrad from the beam axis, the LKr calorimeter is complemented by annular lead glass detectors (LAV) installed in 12 positions inside and downstream of the vacuum tank, and two lead/scintillator sampling calorimeters (IRC, SAC) located close to the beam axis. An iron/scintillator sampling hadronic calorimeter formed of two modules (MUV1,2) and a muon detector consisting of 148 scintillator tiles located behind an 80 cm thick iron wall (MUV3) are used for particle identification.

The data sample analysed is obtained from 8.3×10^5 SPS spills recorded in 2017–2018, with the typical beam intensity increasing over time from 1.8×10^{12} to 2.2×10^{12} protons per spill. The latter value corresponds to a 500 MHz mean beam particle rate at the FV entrance, and a 3.7 MHz mean K^+ decay rate in the FV. The main trigger line is designed for the measurement of the ultra-rare $K^+ \to \pi^+ \nu \bar{\nu}$ decay [14]. The analysis presented here is based on dedicated electron multi-track (eMT) and multi-track (MT) trigger lines operating concurrently with the main trigger line [15, 16], typically downscaled by factors of 8 and 100, respectively. Both trigger lines involve a low-level stage and a high-level stage. The low-level (L0) hardware trigger is based on RICH signal multiplicity and coincidence of signals in two diagonally opposite CHOD quadrants, with an additional requirement of at least 20 GeV deposited in the LKr calorimeter in the eMT line. The high-level (L1) software trigger involves beam K^+ identification by the KTAG and reconstruction of a negatively-charged STRAW track.

Monte Carlo (MC) simulation of particle interactions with the detector and its response is performed using a software package based on the GEANT4 toolkit [17]. Accidental activity and trigger line response are included in the simulation.

2 Event selection

The $K_{2\pi DD}$ events collected concurrently with signal candidates with the same trigger lines are used for normalisation. Signal and normalisation decay modes have the same set of particles in the final state, leading to a first-order cancellation of detector and trigger inefficiencies.

Five-track decays often produce final states with multiple tracks not fully contained in the geometric acceptance of the downstream detectors. The effect is particularly pronounced for the $K_{\pi 4e}$ and $K_{2\pi DD}$ decays which typically produce soft, almost collinear electrons. For example, requiring a fully reconstructed five-track vertex leads to an acceptance of 1.2% for the $K_{2\pi DD}$ decay, and requiring track separation in the STRAW1 plane decreases the acceptance by another order of magnitude, which determines the overall acceptance level.

Only 11% of the $K_{2\pi DD}$ decays with a fully reconstructed five-track vertex have all tracks in the CHOD's geometric acceptance. To avoid an order-of-magnitude loss of acceptance, the analysis relies on the STRAW information only, and the STRAW tracks are not required to be in the geometric acceptance of any downstream detectors. The reduction in selectivity caused by the lack of information from the downstream detectors is mitigated by the exploitation of kinematic constraints on the five-track final state. Main selection criteria are described below.

Five-track vertices compatible with $K_{\pi 4e}$ and $K_{2\pi DD}$ decays are selected as follows:

- Vertices are reconstructed by extrapolating STRAW tracks backward, taking into account the measured residual magnetic field in the vacuum tank. Exactly one five-track vertex should be present in the event within the FV. The longitudinal position of the vertex along the beam axis, z_{vtx}, should be at least 5 m downstream of the start of the FV. The total electric charge of the five tracks should be $q = +1$, their momenta should be in the range 5–45 GeV/c, and their trajectories through the STRAW chambers should be within the respective geometric acceptances. To suppress photon conversions and fake tracks, each pair of tracks should be separated by at least 15 mm in each STRAW chamber plane.

- The momentum excess defined as $\Delta p = p_{vtx} - p_{beam}$, where p_{vtx} is the total momentum of the five tracks and p_{beam} is the central beam momentum, should satisfy $|\Delta p| < 2$ GeV/c. The total transverse momentum of the tracks with respect to the beam axis should be $p_T < 25$ MeV/c. The quantity p_{beam} and the beam axis direction are monitored throughout the data taking, typically every few hours, with $K^+ \to \pi^+\pi^+\pi^-$ decays.

- Track times are evaluated using the STRAW information, with a resolution of 6 ns. Each track is required to be within 20 ns of the trigger time.

Particle identification is based on event kinematics, and is applied as follows:

- The $K^+ \to \pi^+ e^+ e^- e^+ e^-$ final state involves three positively charged tracks (one π^+ and two e^+), and two negatively charged tracks (two e^-). Three assignments of the π^+ mass to one of the positively charged tracks are considered. In each mass assignment, the five-track mass, $m_{\pi 4e}$, the four-electron mass, m_{4e}, and the squared missing mass, $m_{miss}^2 = (P_K - P_\pi)^2$, are evaluated, where P_K is the kaon four-momentum computed using the central beam momentum, and P_π is the reconstructed π^+ four-momentum.

- The mass assignment corresponding to the minimal value of $|m_{\pi 4e} - m_K|$ is chosen, where m_K is the K^+ mass, and it is required that 484 MeV/$c^2 < m_{\pi 4e} < 504$ MeV/c^2. The resolution of $m_{\pi 4e}$ is 1.7 MeV/c^2. The probability of incorrectly assigning the mass is determined by simulation and found to be 4.5% for $K_{\pi 4e}$ decays after the full selection, and $\mathcal{O}(10^{-4})$ for $K_{2\pi DD}$ decays after the full selection which involves a π^0 mass constraint.

The following condition is specific to $K_{2\pi\text{DD}}$ selection:

- For the mass assignment chosen, it is required that $|m_{4e} - m_{\pi^0}| < 10$ MeV/c^2, where m_{π^0} is the π^0 mass. The resolution of m_{4e} is 0.9 MeV/c^2.

The following criteria are specific to $K_{\pi 4e}$ selection:

- To reject events consistent with a $K_{2\pi\text{DD}}$ decay in any mass assignment, the requirements $|m_{4e} - m_{\pi^0}| > 10$ MeV/c^2, $m_{\text{miss}}^2 > 0$ and $|m_{\text{miss}} - m_{\pi^0}| > 40$ MeV/c^2 are applied for all three mass assignments. This reduces the $K_{\pi 4e}$ acceptance by a factor of 0.74.

- To suppress the $K^+ \to \pi^+ \pi_D^0 \pi_D^0$ background, which predominantly enters by incorrect mass assignment (with a soft e^+ from a $\pi_D^0 \to \gamma e^+ e^-$ decay considered as the π^+ candidate), the reconstructed π^+ momentum is required to be $p_\pi > 10$ GeV/c. This reduces the $K_{\pi 4e}$ acceptance by a factor of 0.93.

Selection of the $K_{\pi aa}$ and $K_{\pi S}$ decay chains consists of the $K_{\pi 4e}$ selection with the following additional criteria:

- Two $X \to e^+ e^-$ decay hypotheses are examined for the four $e^\pm$ candidates in the mass assignment chosen. In each hypothesis, the masses of the two $e^+ e^-$ pairs, m_{ee1} and m_{ee2}, are evaluated, and a discriminant is computed to quantify the consistency of the two mass values:

$$\mathcal{D} = (m_{ee1} - m_{ee2})^2 / (4.9 \times 10^{-3} \cdot m_{ee})^2.$$

  Here $m_{ee} = (m_{ee1} + m_{ee2})/2$ is the reconstructed mass of the intermediate particle X which is pair-produced, and the denominator represents the squared resolution of the quantity $m_{ee1} - m_{ee2}$, evaluated with simulation and found to be proportional to m_{ee}. The $X \to e^+ e^-$ hypothesis with the smaller $\mathcal{D}$ value is considered, and it is required that $\mathcal{D} < 9$ in this hypothesis.

- For each X mass hypothesis (m_X), it is required that $|m_{ee} - m_X| < 0.02 \cdot m_X$.

The signal region in the data is kept masked until the completion and validation of the background evaluation.

3 Number of kaon decays in the fiducial volume

The reconstructed $m_{\pi 4e}$ distributions of $K_{2\pi\text{DD}}$ candidates from both data and simulation are displayed in Fig. 2. The simulation reproduces the gaussian part of the $m_{\pi 4e}$ spectrum but does not fully describe the radiative tail; this is due to a soft-photon bremsstrahlung approximation [18] used to model the radiative corrections to the π_{DD}^0 decay.

The number of K^+ decays in the FV is computed as

$$N_K = \frac{f \cdot N_{\text{DD}}}{\mathcal{B}(K_{2\pi}) \cdot \mathcal{B}(\pi_{\text{DD}}^0) \cdot A_{\text{DD}}} = (8.58 \pm 0.19_{\text{stat}} \pm 0.07_{\text{MC}} \pm 0.41_{\text{ext}}) \times 10^{11},$$

where $N_{\text{DD}} = 2023$ is the number of $K_{2\pi\text{DD}}$ candidates in the data; $\mathcal{B}(K_{2\pi}) = (20.67 \pm 0.08) \times 10^{-2}$ and $\mathcal{B}(\pi_{\text{DD}}^0) = (3.34 \pm 0.16) \times 10^{-5}$ are the $K^+ \to \pi^+ \pi^0$ and π_{DD}^0 decay branching ratios [5]; $A_{\text{DD}} = (3.41 \pm 0.02_{\text{stat}} \pm 0.02_{\text{syst}}) \times 10^{-4}$ is the acceptance of the $K_{2\pi\text{DD}}$ selection evaluated with simulation (the systematic error is evaluated by variation of the $m_{\pi 4e}$ selection conditions); $f = 0.9987$ is the purity of the $K_{2\pi\text{DD}}$ sample evaluated with simulation and accounting for the $K^+ \to \pi_{\text{DD}}^0 \ell^+ \nu$ background ($\ell = e, \mu$). The three uncertainties quoted in N_K arise from the limited size of the data sample, the total uncertainty in the acceptance A_{DD}, and the external uncertainties in the measured values of $\mathcal{B}(K_{2\pi})$ and $\mathcal{B}(\pi_{\text{DD}}^0)$.
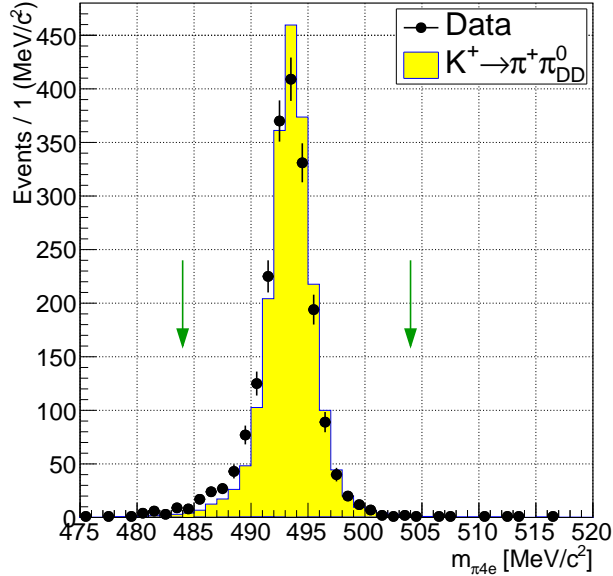
Figure 2: Reconstructed $m_{\pi 4e}$ spectra for the data and a simulated $K_{2\pi\mathrm{DD}}$ sample obtained with the $K_{2\pi\mathrm{DD}}$ selection. The signal mass region is indicated by vertical arrows.

The acceptance A_{DD} includes the effects of accidental activity and trigger efficiencies. The efficiencies of the CHOD and LKr trigger conditions for the $K_{2\pi\mathrm{DD}}$ sample are found with simulation to be 74% and 81% respectively, and are relatively low due to the absence of the CHOD and LKr geometric acceptance requirements for the tracks. The efficiencies of the RICH, KTAG and STRAW trigger conditions exceed 99%.

4 Background estimation

Background from five-track and seven-track K^+ decays is evaluated with simulation; all K^+ decays with branching ratios exceeding 10^{-8} are considered. Background from coincidences of pairs of three-track K^+ decays in time (with one track not reconstructed) is evaluated with dedicated simulation of pairs of decays occurring within 25 ns; coincidences of all types of three-track K^+ decays with products of branching ratios exceeding 2×10^{-6} are considered. The probability of two decays occurring within this 25 ns time window is dependent upon the instantaneous beam intensity, and is accounted for by normalising the total estimated background to the data in the momentum excess region $\Delta p > 20$ GeV/c.

Contributions from all possible triple coincidences of one or more $K^+ \to \pi^+\pi^+\pi^-$ decays with $K^+ \to \mu^+\nu$ decays and beam halo particles, and contributions from coincidences of three-track decays with inelastic interactions of beam particles in GTK3, are found to be much smaller than those from coincidences of pairs of three-track decays, and are neglected.

The reconstructed momentum excess (Δp) and five-track mass ($m_{\pi 4e}$) spectra for data and simulated events after the $K_{\pi 4e}$ selection are shown in Fig. 3. The region of large Δp values is dominated by backgrounds from coincidences of three-track decays. The integrals of the data and simulated spectra agree in the region $\Delta p > 20$ GeV/c by construction. The region $\Delta p < 0$ is dominated by backgrounds from single five-track decays which, with the exception of the $K_{2\pi\mathrm{DD}}$ decay, lead to photons and neutrinos in the final state.

The background model is validated against the data in the control region $\Delta p < -2$ GeV/c using the standard $K_{\pi 4e}$ selection (Fig. 3, left) and a loose $K_{\pi 4e}$ selection with the condition $p_\pi > 10$ GeV/c removed. The results are shown in Table 1. The loose selection leads to a sharp increase in the $K^+ \to \pi^+\pi_{\mathrm{D}}^0\pi_{\mathrm{D}}^0$ background in the control region due to the soft momentum spectrum of the positrons from π_{D}^0 decays misidentified as π^+ (Section 2).
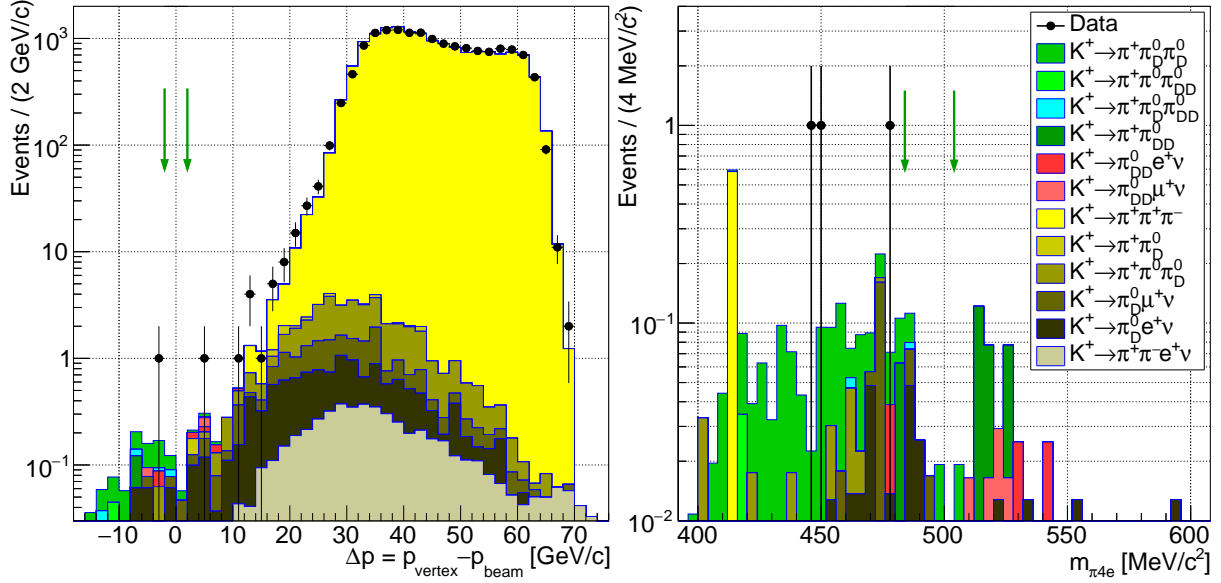
6

Figure 3: Reconstructed momentum excess (Δp, left) and five-track mass ($m_{\pi 4e}$, right) spectra for data and simulated samples after the $K_{\pi 4e}$ selection obtained by removing the Δp condition (left panel) or the $m_{\pi 4e}$ condition (right panel). Contributions from three-track K^+ decays (the last six entries in the legend) are due to coincidences with a $K^+ \to \pi^+\pi^+\pi^-$ decay. The sum of these contributions is normalised to the data in the region $\Delta p > 20$ GeV/c. The signal region is shown with pairs of vertical arrows in both plots.

Table 1: Backgrounds to the $K_{\pi 4e}$ decay, their branching ratios (or products of branching ratios for coincidences of two decays), and estimated backgrounds with their statistical uncertainties in the control ($\Delta p < -2$ GeV/c) and signal ($|\Delta p| < 2$ GeV/c) momentum excess regions shown in Fig. 3 (left). Estimated backgrounds in the control region for a loose $K_{\pi 4e}$ selection, with the $p_\pi > 10$ GeV/c condition removed, are also shown. The $K^+ \to \pi^+\pi^0_D e^+e^-$ decay, as well as the $K^+ \to \pi^+\pi^- e^+\nu$ decay in coincidence with a $K^+ \to \pi^+\pi^+\pi^-$ decay, and coincidences of any of the two decays, $K^+ \to \pi^+\pi^+\pi^-$ and $K^+ \to \pi^+\pi^0_D$, lead to negligible backgrounds in the control and signal regions, and are not listed.

Source	Branching ratio (or their product)	Control region	Control region, loose selection	Signal region
Single five-track and seven-track decays				
$K_{2\pi DD}$	6.9×10^{-6}	0.06 ± 0.06	0.06 ± 0.06	–
$K^+ \to \pi^+\pi^0_D\pi^0_D$	2.4×10^{-6}	0.30 ± 0.06	2.47 ± 0.16	0.04 ± 0.02
$K^+ \to \pi^0_{DD} e^+\nu$	1.7×10^{-6}	0.10 ± 0.05	0.10 ± 0.05	–
$K^+ \to \pi^+\pi^0\pi^0_{DD}$	1.2×10^{-6}	0.03 ± 0.03	0.03 ± 0.03	–
$K^+ \to \pi^0_{DD}\mu^+\nu$	1.1×10^{-6}	0.02 ± 0.02	0.03 ± 0.02	–
$K^+ \to \pi^+\pi^0_D\pi^0_{DD}$	1.4×10^{-8}	0.05 ± 0.02	0.10 ± 0.02	0.01 ± 0.01
Coincidences of three-track decays with a $K^+ \to \pi^+\pi^+\pi^-$ decay				
$K^+ \to \pi^0_D e^+\nu$	3.3×10^{-5}	0.15 ± 0.07	0.15 ± 0.07	0.08 ± 0.05
$K^+ \to \pi^+\pi^0\pi^0_D$	2.3×10^{-5}	0.03 ± 0.03	0.08 ± 0.05	–
$K^+ \to \pi^0_D\mu^+\nu$	2.2×10^{-5}	0.03 ± 0.02	0.04 ± 0.02	0.05 ± 0.02
Total		0.77 ± 0.13	3.06 ± 0.21	0.18 ± 0.06
Data		1	4	0

The background model is further validated using the $m_{\pi 4e}$ spectrum outside the signal region. Using the standard $K_{\pi 4e}$ selection, three data events are observed with an expected background of $2.83\pm0.64_{\mathrm{stat}}$ (Fig. 3, right); using the loose $K_{\pi 4e}$ selection, five data events are observed with an expected background of $3.99\pm0.74_{\mathrm{stat}}$. In all cases, the data are in agreement with simulation within statistical fluctuations, and the largest background comes from the $K^+ \to \pi^+\pi_{\mathrm{D}}^0\pi_{\mathrm{D}}^0$ decay.

The background contributions in the signal region after the $K_{\pi 4e}$ selection are summarised in Table 1. The estimate of the total background, validated by agreement of the data with simulation in the control regions, is

$$N_B = 0.18 \pm 0.06_{\mathrm{stat}} \pm 0.13_{\mathrm{syst}} = 0.18 \pm 0.14,$$

where a 100% relative systematic uncertainty is assigned to the contribution from coincidences of three-track decays, based on the level of agreement of data and simulation in the momentum excess region $2\ \mathrm{GeV}/c < \Delta p < 20\ \mathrm{GeV}/c$.

The requirement that the two reconstructed e^+e^- masses (m_{ee1}, m_{ee2}) are consistent with each other, applied in the selection of the $K_{\pi aa}$ and $K_{\pi S}$ decay chains, leads to a reduction of the background with respect to the $K_{\pi 4e}$ selection. The probability of the reconstructed m_{ee1} and m_{ee2} values being consistent is found to be 2% in simulated samples of $K^+ \to \pi^+\pi_{\mathrm{D}}^0\pi_{\mathrm{D}}^0$ and $K^+ \to \pi^+\pi_{\mathrm{DD}}^0$ decays. Furthermore, the probability of $|m_{ee} - m_X| < 0.02 \cdot m_X$ for the above samples does not exceed 10% in any m_X hypothesis considered (where $X = a, A'$) as established with simulations. The background to the $K_{\pi aa}$ and $K_{\pi S}$ processes in each m_X hypothesis is estimated as

$$N_B' = (0.4 \pm 0.4) \times 10^{-3},$$

where a 100% relative uncertainty is conservatively assigned.

5 Search for the signal decays

The $K_{\pi 4e}$ decay is modelled according to the SM description [6]. The non-resonant part of the decay amplitude is considered, including the dominant one-photon exchange diagram ($K^+ \to \pi^+\gamma^*$), the two-photon exchange diagram ($K^+ \to \pi^+\gamma^*\gamma^*$), and their interference. The contribution from the π^0 pole in the two-photon exchange is neglected; it does not interfere with the other amplitudes, peaks at $m_{4e} \approx m_{\pi^0}$, and accounts for 3% of the total decay rate in the region $|m_{4e} - m_{\pi^0}| > 10\ \mathrm{MeV}/c^2$ used in this analysis. The acceptance of the $K_{\pi 4e}$ selection for the $K_{\pi 4e}$ signal is found to be $A_{\pi 4e} = (1.85 \pm 0.06_{\mathrm{stat}}) \times 10^{-4}$.

The prompt decay chain $K^+ \to \pi^+aa$, $a \to e^+e^-$, allowed kinematically for axion masses in the range $2m_e \leq m_a \leq (m_K - m_\pi)/2$, is simulated with a uniform $K^+ \to \pi^+aa$ phase-space distribution [3] and isotropic $a \to e^+e^-$ decays, for 33 equally-spaced m_a hypotheses in the range 10–170 MeV/c^2. The acceptance of the $K_{\pi aa}$ selection reaches a maximum of 7.1×10^{-3} for $m_a = 155\ \mathrm{MeV}/c^2$.

The prompt decay chain $K^+ \to \pi^+S$, $S \to A'A'$, $A' \to e^+e^-$, allowed kinematically in the mass region $2m_e \leq m_{A'} \leq m_S/2 \leq (m_K - m_\pi)/2$, is simulated as a series of isotropic decays for $m_{A'}$ hypotheses in the range 10–170 MeV/c^2 and m_S hypotheses in the range 20–340 MeV/c^2, with a 5 MeV/c^2 step in both $m_{A'}$ and m_S. The region 120 $\mathrm{MeV}/c^2 < m_S < 165\ \mathrm{MeV}/c^2$ is excluded from the search as the signal acceptance is suppressed in this region by the selection conditions that reduce the $K_{2\pi\mathrm{DD}}$ background. The acceptance of the $K_{\pi S}$ selection reaches a maximum of 1.1×10^{-2} at the kinematic boundary for $m_{A'} = 150\ \mathrm{MeV}/c^2$ and $m_S = 300\ \mathrm{MeV}/c^2$.

The $K_{\pi aa}$ and $K_{\pi S}$ decays typically produce energetic, well-separated electrons in the final state, which leads to significantly larger acceptances than for $K_{\pi 4e}$ and $K_{2\pi\mathrm{DD}}$ decays.
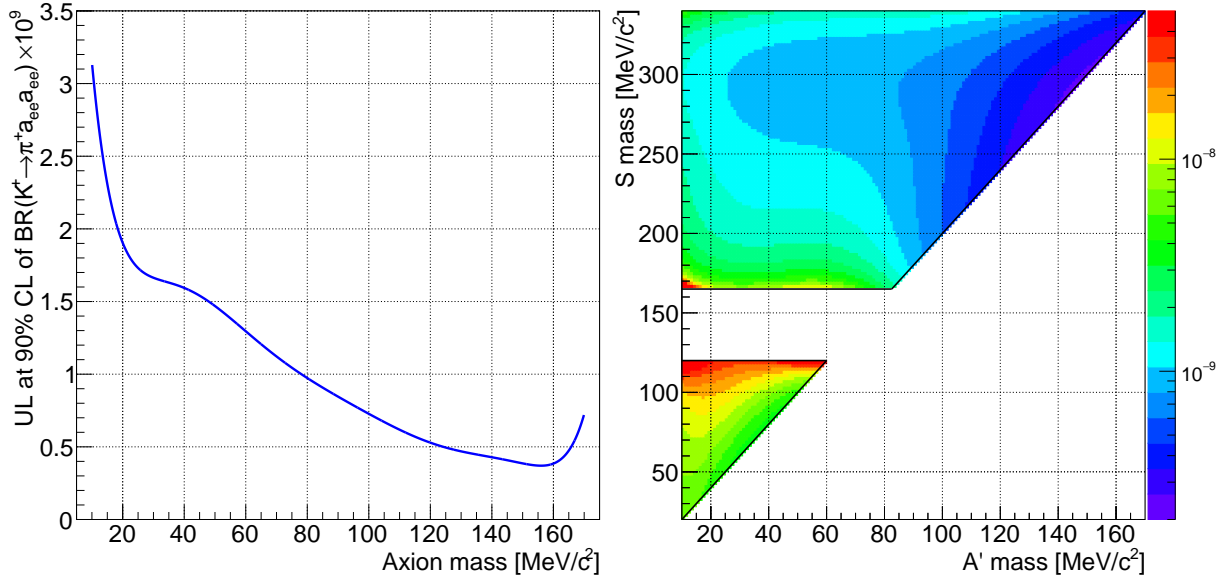
Figure 4: Left: upper limit at 90% CL of the branching ratio of the prompt decay chain $K^+ \to \pi^+ aa$, $a \to e^+e^-$ as a function of the assumed axion mass. Right: upper limit at 90% CL of the branching ratio of the prompt decay chain $K^+ \to \pi^+ S$, $S \to A'A'$, $A' \to e^+e^-$ as a function of the assumed dark-photon and dark-scalar masses. Discrete sets of points obtained with a step size of 5 MeV/c^2 are approximated by polynomial functions in each case.

6 Results

No data events are observed in the signal region after unmasking. In this case, upper limits at 90% CL on the signal branching ratios computed using the CL$_S$ method [19] do not depend on the expected background and are equal to $2.3/(A\,N_K)$, where A denotes the signal acceptance. The uncertainties in N_K and signal acceptances are taken into account in the CL$_S$ procedure. An upper limit of $\mathcal{B}(K_{\pi 4e}) < 1.4 \times 10^{-8}$ is established at 90% CL for the branching ratio of the non-resonant part of the $K_{\pi 4e}$ decay, which is a factor 200 larger than the SM expectation [6].

Upper limits obtained at 90% CL for the branching ratios of the $K_{\pi aa}$ and $K_{\pi S}$ decay chains are shown as functions of the assumed masses of the dark-sector mediators in Fig. 4. For the product $\mathcal{B}(K^+ \to \pi^+ aa) \times [\mathcal{B}(a \to e^+e^-)]^2$, the most stringent upper limit of 3.7×10^{-10} is obtained for $m_a = 155$ MeV/c^2. The upper limit of 2.1×10^{-9} obtained for the above quantity for $m_a = 17$ MeV/c^2 excludes the QCD axion explanation of the "17 MeV anomaly" in the mass spectra of the e^+e^- pairs produced in nuclear de-excitation [10, 11, 12], according to the decay rate estimate reported in Ref. [3]. For the product $\mathcal{B}(K^+ \to \pi^+ S) \times \mathcal{B}(S \to A'A') \times [\mathcal{B}(A' \to e^+e^-)]^2$, the most stringent upper limit of 2.5×10^{-10} is obtained for $m_{A'} = 150$ MeV/c^2 and $m_S = 300$ MeV/c^2.

Summary

The first search for ultra-rare K^+ decays into the $\pi^+ e^+e^-e^+e^-$ final state is reported, using a dataset collected by the NA62 experiment at CERN in 2017–2018. An upper limit of 1.4×10^{-8} at 90% CL is obtained for the branching ratio of the $K^+ \to \pi^+ e^+e^-e^+e^-$ decay, with the expected SM branching ratio of $(7.2 \pm 0.7) \times 10^{-11}$. Upper limits at 90% CL are obtained at the level of 10^{-9} for the branching ratios of two prompt decay chains involving pair-production of hidden-sector mediators: $K^+ \to \pi^+ aa$, $a \to e^+e^-$ and $K^+ \to \pi^+ S$, $S \to A'A'$, $A' \to e^+e^-$. The QCD axion is excluded as a possible explanation of the "17 MeV anomaly" according to the decay rate estimate reported in Ref. [3].

Acknowledgements

References

[1] J. Beacham *et al.*, J. Phys. **G47** (2020) 010501.

[2] P. Agrawal *et al.*, Eur. Phys. J. **C81** (2021) 11.

[3] M. Hostert and M. Pospelov, Phys. Rev. **D105** (2022) 015017.

[4] E. Goudzovski *et al.*, Rep. Prog. Phys. **86** (2023) 016201.

[5] R.L. Workman *et al.*, Prog. Theor. Exp. Phys. **2022** (2022) 083C01.

[6] T. Husek, Phys. Rev. **D106** (2022) L071301.

[7] D. Alves and N. Weiner, JHEP **07** (2018) 092.

[8] D. Alves, Phys. Rev. **D103** (2021) 055018.

[9] D. Alves *et al.*, Eur. Phys. J. **C83** (2023) 230.

[10] A.J. Krasznahorkay *et al.*, Phys. Rev. Lett. **116** (2016) 042501.

[11] A.J. Krasznahorkay *et al.*, Phys. Rev. **C104** (2021) 044003.

[12] A.J. Krasznahorkay *et al.*, Phys. Rev. **C106** (2022) L061601.

[13] E. Cortina Gil *et al.*, JINST **12** (2017) P05025.

[14] E. Cortina Gil *et al.*, JHEP **06** (2021) 93.

[15] R. Ammendola *et al.*, Nucl. Instrum. Methods **A929** (2019) 1.

[16] E. Cortina Gil *et al.*, JHEP **03** (2023) 122.

[17] J. Allison *et al.*, Nucl. Instrum. Methods **A835** (2016) 186.

[18] K. Kampf, J. Novotný and P. Sanchez-Puertas, Phys. Rev. **D97** (2018) 056010.

[19] A.L. Read, J. Phys. **G28** (2002) 2693.

The NA62 Collaboration

Université Catholique de Louvain, Louvain-La-Neuve, Belgium
E. Cortina Gil, A. Kleimenova [1], E. Minucci [2], S. Padolski, P. Petrov, A. Shaikhiev [3], R. Volpe [4]

TRIUMF, Vancouver, British Columbia, Canada
T. Numao, Y. Petrov, B. Velghe, V. W. S. Wong

University of British Columbia, Vancouver, British Columbia, Canada
D. Bryman [5], J. Fu

Charles University, Prague, Czech Republic
Z. Hives, T. Husek, J. Jerhot [6], K. Kampf, M. Zamkovsky [7]

Aix Marseille University, CNRS/IN2P3, CPPM, Marseille, France
B. De Martino, M. Perrin-Terrin

Institut für Physik and PRISMA Cluster of Excellence, Universität Mainz, Mainz, Germany
A.T. Akmete, R. Aliberti [8], G. Khoriauli [9], J. Kunze, D. Lomidze [10], L. Peruzzo, M. Vormstein, R. Wanke

Dipartimento di Fisica e Scienze della Terra dell'Università e INFN, Sezione di Ferrara, Ferrara, Italy
P. Dalpiaz, M. Fiorini, A. Mazzolari, I. Neri, A. Norton [11], F. Petrucci, M. Soldani, H. Wahl [12]

INFN, Sezione di Ferrara, Ferrara, Italy
L. Bandiera, A. Cotta Ramusino, A. Gianoli, M. Romagnoni, A. Sytov

Dipartimento di Fisica e Astronomia dell'Università e INFN, Sezione di Firenze, Sesto Fiorentino, Italy
E. Iacopini, G. Latino, M. Lenti, P. Lo Chiatto, I. Panichi, A. Parenti

INFN, Sezione di Firenze, Sesto Fiorentino, Italy
A. Bizzeti [13], F. Bucci

Laboratori Nazionali di Frascati, Frascati, Italy
A. Antonelli, G. Georgiev [14], V. Kozhuharov [14], G. Lanfranchi, S. Martellotti, M. Moulson, T. Spadaro, G. Tinti

Dipartimento di Fisica "Ettore Pancini" e INFN, Sezione di Napoli, Napoli, Italy
F. Ambrosino, T. Capussela, M. Corvino, M. D'Errico, D. Di Filippo, R. Fiorenza [15], R. Giordano, P. Massarotti, M. Mirra, M. Napolitano, I. Rosa, G. Saracino

Dipartimento di Fisica e Geologia dell'Università e INFN, Sezione di Perugia, Perugia, Italy
G. Anzivino, F. Brizioli [7], E. Imbergamo, R. Lollini, R. Piandani [16], C. Santoni

INFN, Sezione di Perugia, Perugia, Italy

M. Barbanera, P. Cenci, B. Checcucci, P. Lubrano, M. Lupi [17], M. Pepe, M. Piccini

Dipartimento di Fisica dell'Università e INFN, Sezione di Pisa, Pisa, Italy

F. Costantini, L. Di Lella [12], N. Doble [12], M. Giorgi, S. Giudici, G. Lamanna, E. Lari, E. Pedreschi, M. Sozzi

INFN, Sezione di Pisa, Pisa, Italy

C. Cerri, R. Fantechi, L. Pontisso [18], F. Spinella

Scuola Normale Superiore e INFN, Sezione di Pisa, Pisa, Italy

I. Mannelli

Dipartimento di Fisica, Sapienza Università di Roma e INFN, Sezione di Roma I, Roma, Italy

G. D'Agostini, M. Raggi

INFN, Sezione di Roma I, Roma, Italy

A. Biagioni, P. Cretaro, O. Frezza, E. Leonardi, A. Lonardo, M. Turisini, P. Valente, P. Vicini

INFN, Sezione di Roma Tor Vergata, Roma, Italy

R. Ammendola, V. Bonaiuto [19], A. Fucci, A. Salamon, F. Sargeni [20]

Dipartimento di Fisica dell'Università e INFN, Sezione di Torino, Torino, Italy

R. Arcidiacono [21], B. Bloch-Devaux, M. Boretto [7], E. Menichetti, E. Migliore, D. Soldi

INFN, Sezione di Torino, Torino, Italy

C. Biino, A. Filippi, F. Marchetto

Instituto de Física, Universidad Autónoma de San Luis Potosí, San Luis Potosí, Mexico

A. Briano Olvera, J. Engelfried, N. Estrada-Tristan [22], M. A. Reyes Santos [22]

Horia Hulubei National Institute for R&D in Physics and Nuclear Engineering, Bucharest-Magurele, Romania

P. Boboc, A. M. Bragadireanu, S. A. Ghinescu, O. E. Hutanu

Faculty of Mathematics, Physics and Informatics, Comenius University, Bratislava, Slovakia

L. Bician [23], T. Blazek, V. Cerny, Z. Kucerova [7]

CERN, European Organization for Nuclear Research, Geneva, Switzerland

J. Bernhard, A. Ceccucci, M. Ceoletta, H. Danielsson, N. De Simone [24], F. Duval, B. Döbrich [25], L. Federici, E. Gamberini, L. Gatignon [3], R. Guida, F. Hahn [†], E. B. Holzer, B. Jenninger, M. Koval [23], P. Laycock [26], G. Lehmann Miotto, P. Lichard, A. Mapelli, R. Marchevski [1], K. Massri, M. Noy, V. Palladino, J. Pinzino [27], V. Ryjov, S. Schuchmann, S. Venditti

School of Physics and Astronomy, University of Birmingham, Birmingham, United Kingdom

T. Bache, M. B. Brunetti [28], V. Duk [4], V. Fascianelli [29], J. R. Fry, F. Gonnella, E. Goudzovski [*], J. Henshaw, L. Iacobuzio, C. Kenworthy, C. Lazzeroni, N. Lurkin [6], F. Newson, C. Parkinson, A. Romano, J. Sanders, A. Sergi [30], A. Sturgess, J. Swallow [7], A. Tomczak

School of Physics, University of Bristol, Bristol, United Kingdom

H. Heath, R. Page, S. Trilov

School of Physics and Astronomy, University of Glasgow, Glasgow, United Kingdom

B. Angelucci, D. Britton, C. Graham, D. Protopopescu

Faculty of Science and Technology, University of Lancaster, Lancaster, United Kingdom

J. Carmignani [31], J. B. Dainton, R. W. L. Jones, G. Ruggiero [32]

School of Physical Sciences, University of Liverpool, Liverpool, United Kingdom

L. Fulton, D. Hutchcroft, E. Maurice [33], B. Wrona

Physics and Astronomy Department, George Mason University, Fairfax, Virginia, USA

A. Conovaloff, P. Cooper, D. Coward [34], P. Rubin

Authors affiliated with an Institute or an international laboratory covered by a cooperation agreement with CERN

A. Baeva, D. Baigarashev [35], D. Emelyanov, T. Enik, V. Falaleev [4], S. Fedotov, K. Gorshanov, E. Gushchin, V. Kekelidze, D. Kereibay, S. Kholodenko [27], A. Khotyantsev, A. Korotkova, Y. Kudenko, V. Kurochka, V. Kurshetsov, L. Litov [14], D. Madigozhin, M. Medvedeva, A. Mefodev, M. Misheva [36], N. Molokanova, S. Movchan, V. Obraztsov, A. Okhotnikov, A. Ostankov [†], I. Polenkevich, Yu. Potrebenikov, A. Sadovskiy, V. Semenov [†], S. Shkarovskiy, V. Sugonyaev, O. Yushchenko, A. Zinchenko [†]

[*] Corresponding author: E. Goudzovski, email: evgueni.goudzovski@cern.ch

[†] Deceased

[1] Present address: Ecole Polytechnique Fédérale Lausanne, CH-1015 Lausanne, Switzerland

[2] Present address: Syracuse University, Syracuse, NY 13244, USA

[3] Present address: Faculty of Science and Technology, University of Lancaster, Lancaster, LA1 4YW, UK

[4] Present address: INFN, Sezione di Perugia, I-06100 Perugia, Italy

[5] Also at TRIUMF, Vancouver, British Columbia, V6T 2A3, Canada

[6] Present address: Université Catholique de Louvain, B-1348 Louvain-La-Neuve, Belgium

[7] Present address: CERN, European Organization for Nuclear Research, CH-1211 Geneva 23, Switzerland

[8] Present address: Institut für Kernphysik and Helmholtz Institute Mainz, Universität Mainz, Mainz, D-55099, Germany

[9] Present address: Universität Würzburg, D-97070 Würzburg, Germany

[10]Present address: European XFEL GmbH, D-22869 Schenefeld, Germany

[11]Present address: School of Physics and Astronomy, University of Glasgow, Glasgow, G12 8QQ, UK

[12]Present address: Institut für Physik and PRISMA Cluster of Excellence, Universität Mainz, D-55099 Mainz, Germany

[13]Also at Dipartimento di Scienze Fisiche, Informatiche e Matematiche, Università di Modena e Reggio Emilia, I-41125 Modena, Italy

[14]Also at Faculty of Physics, University of Sofia, BG-1164 Sofia, Bulgaria

[15]Present address: Scuola Superiore Meridionale e INFN, Sezione di Napoli, I-80138 Napoli, Italy

[16]Present address: Instituto de Física, Universidad Autónoma de San Luis Potosí, 78240 San Luis Potosí, Mexico

[17]Present address: Institut am Fachbereich Informatik und Mathematik, Goethe Universität, D-60323 Frankfurt am Main, Germany

[18]Present address: INFN, Sezione di Roma I, I-00185 Roma, Italy

[19]Also at Department of Industrial Engineering, University of Roma Tor Vergata, I-00173 Roma, Italy

[20]Also at Department of Electronic Engineering, University of Roma Tor Vergata, I-00173 Roma, Italy

[21]Also at Università degli Studi del Piemonte Orientale, I-13100 Vercelli, Italy

[22]Also at Universidad de Guanajuato, 36000 Guanajuato, Mexico

[23]Present address: Charles University, 116 36 Prague 1, Czech Republic

[24]Present address: DESY, D-15738 Zeuthen, Germany

[25]Present address: Max-Planck-Institut für Physik (Werner-Heisenberg-Institut), München, D-80805, Germany

[26]Present address: Brookhaven National Laboratory, Upton, NY 11973, USA

[27]Present address: INFN, Sezione di Pisa, I-56100 Pisa, Italy

[28]Present address: Department of Physics, University of Warwick, Coventry, CV4 7AL, UK

[29]Present address: Center for theoretical neuroscience, Columbia University, New York, NY 10027, USA

[30]Present address: Dipartimento di Fisica dell'Università e INFN, Sezione di Genova, I-16146 Genova, Italy

[31]Present address: School of Physical Sciences, University of Liverpool, Liverpool, L69 7ZE, UK

[32]Present address: Dipartimento di Fisica e Astronomia dell'Università e INFN, Sezione di Firenze, I-50019 Sesto Fiorentino, Italy

[33]Present address: Laboratoire Leprince Ringuet, F-91120 Palaiseau, France

[34]Also at SLAC National Accelerator Laboratory, Stanford University, Menlo Park, CA 94025, USA

[35]Also at L.N. Gumilyov Eurasian National University, 010000 Nur-Sultan, Kazakhstan

[36]Present address: Institute of Nuclear Research and Nuclear Energy of Bulgarian Academy of Science (INRNE-BAS), BG-1784 Sofia, Bulgaria